

Importance of Bimolecular Interactions in Developing Empirical Potential Functions for Liquid Ammonia

Jiali Gao,* Xinfu Xia, and Thomas F. George†

Department of Chemistry, State University of New York at Buffalo, Buffalo, New York 14214

Received: March 15, 1993*

A four-site intermolecular potential function for NH_3 has been developed and tested in Monte Carlo statistical mechanics simulations of the liquid at its boiling point (-33.35°C) and 1 atm. The potential yields good thermodynamic results for liquid ammonia, while the structures of the liquid are characterized through radial distribution functions and hydrogen-bonding analyses. The results indicate that each ammonia forms on average three hydrogen bonds and the liquid contains winding chains of hydrogen bonded monomers. Roughly linear hydrogen bonds predominates in the liquid. The results were also compared with those obtained using the five-site model developed by Ferrario et al. Although the computed heat of vaporization, liquid density, and the radial distribution functions are in good accord with our results and experimental data, to our surprise, a significant difference in the dimer and liquid structures exists between the two theoretical models. The structural difference is due to the occurrence of unrealistic dimer structures with donation of hydrogen bonds to the opposite side of the ammonia lone pair in the liquid from the model of Ferrario et al. In contrast, both *ab initio* calculations and the present four-site model predict no stable complexes for these structures. These findings emphasize the importance of specific consideration of bimolecular interactions in developing potential functions for fluid simulations and suggest that erroneous results might be obtained if the potential functions are fitted to reproduce the condensed-phase properties alone.

Introduction

The traditional notion that hydrogen bonding interactions predominate in liquid ammonia leading to anomalously high melting and boiling point temperatures has been challenged by recent experimental results of dimeric ammonia complex in the gas phase.^{1,2} The experimental results suggest that although ammonia is an excellent proton acceptor, its ability to donate hydrogen bonds is extremely poor.^{2,3} In particular, the results reported by Klemperer and co-workers suggested that the $\text{N}\cdots\text{H}-\text{N}$ angle and the hydrogen-bond distance are at best 120° and 2.64 \AA ,^{2,3} which are far from the ideal values for hydrogen bonds.⁴ Weak interactions in the ammonia dimer were also predicted through analyses of matrix infrared and Raman spectroscopic results.⁵ However, the structure derived from microwave spectroscopy of the NH_3 dimer has been controversial, and recent studies indicate that the ammonia dimer may prefer a linear hydrogen bond.⁶ Parallel to these experimental findings, *ab initio* molecular orbital (MO) calculations predict that the hydrogen-bond-donating ability of NH_3 is much poorer than its accepting ability, while the equilibrium structure consists of a roughly linear hydrogen bond.^{7,8}

In the course of a study of the $\text{S}_{\text{N}}2$ Menshutkin reaction of $\text{NH}_3 + \text{CH}_3\text{Cl} \rightarrow \text{CH}_3\text{NH}_3^+ + \text{Cl}^-$ in solution in our laboratory, the intermolecular potential function for ammonia was needed.⁹ Further, in view of the utility of ammonia as a polar protic solvent and the importance of hydrogen bonding in determining the structure and reactivity of biological systems,^{1,4} a thorough investigation of the liquid using an improved potential is warranted.

There have been several computer simulation studies of liquid ammonia, with encouraging results.¹⁰⁻¹³ However, the intermolecular potential functions used in previous simulations were developed primarily based on *ab initio* results for bimolecular complexes with small basis sets or on experimental condensed-phase properties alone. Since the computed fluid results depend

critically on the potential functions used, it has led us to examine one of the most successful potentials for NH_3 that was introduced by Ferrario et al. (hereafter referred to as the FHMK model).¹² Surprisingly, some structural and energetic features for the ammonia dimer predicted by the FHMK model are significantly different from those obtained through high-level *ab initio* MO calculations, in spite of the fact that the computed condensed phase properties are in good agreement with experiments.^{11,12} Consequently, we decided to derive a new potential function for use in simulations of liquid ammonia, which can also properly describe bimolecular interactions in the gas phase. In this paper structural and energetic results for liquid ammonia obtained with the FHMK potential and the present four-site model are compared. In what follows, we present an interesting example where two empirical potential functions yield virtually identical thermodynamic properties for the pure liquid including the heat of vaporization, density, and radial distribution functions (rdf), all in good accord with the available experimental data, but differing significantly in dimer and liquid structures. The findings of this study emphasize the importance of a coherent consideration of both the gas-phase and condensed-phase properties in the development of empirical potential functions.

Computational Details

Intermolecular Potential Functions. In the present study, the ammonia molecule is represented by four interaction sites located on the nucleus centers. The microwave structure is used and held rigid throughout the fluid simulations.¹⁴ In this model, a positive partial charge (q_{H}) is placed on each hydrogen atom and the negative charge ($-3q_{\text{H}}$) is carried by the nitrogen. It was found that it is not necessary to include an extra virtual interaction site to describe the lone pair of electrons in ammonia. On the other hand, a five-site model was adopted by Ferrario et al.,^{11,12} in which the negative charge is moved off the nitrogen atom by 0.15 \AA in the direction toward the hydrogen atoms along the C_{3v} symmetry axis. This arrangement and the selection of charges were designed to reproduce the experimental gas-phase dipole and quadrupole moments. The structural parameters are summarized in Table I.

* Address correspondence to this author.

† Present address: Departments of Chemistry and Physics, Washington State University, Pullman, WA 99164-1046.

* Abstract published in *Advance ACS Abstracts*, August 15, 1993.

TABLE I: Geometrical Parameters for the Ammonia Molecules Adopted in the Present Four-Site and the FHMK Models^a

model	$R(\text{N-H}), \text{\AA}$	$\angle \text{HNH}, \text{deg}$	$R(\text{N-M}), \text{\AA}$	$\angle \text{HNM}, \text{deg}$
this work	1.0124	106.67		
FHMK	1.0127	110.90	0.15	72.0

^a M is a virtual site on the C_{3v} axis toward the hydrogen atoms in ammonia.

TABLE II: Potential Function Parameters for Ammonia

atom or site	q	$\sigma, \text{\AA}$	$\epsilon, \text{kcal/mol}$
This Work			
N	-1.026	3.36	0.210
H	0.342	0.0	0.0
FHMK Model			
N	0.0	3.40	0.278
H	0.485	0.0	0.0
M	-1.455	0.0	0.0

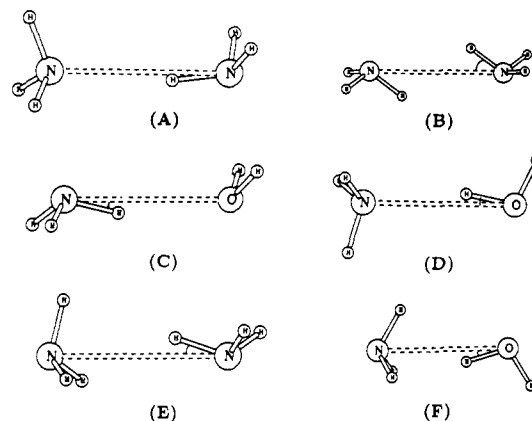
The potential energy between two ammonia molecules m and n , ΔE_{mn} , consists of Coulombic interactions between the charges i on m and the charges j on n plus a Lennard-Jones term between the two nitrogen atoms:

$$\Delta E_{mn} = \sum_{i=1}^{\text{on } m} \sum_{j=1}^{\text{on } n} \frac{q_i q_j e^2}{r_{ij}} + 4\epsilon_N \left[\left(\frac{\sigma_N}{r_{NN}} \right)^{12} - \left(\frac{\sigma_N}{r_{NN}} \right)^6 \right] \quad (1)$$

where r_{ij} and r_{NN} are the separation distances between the charged sites and nitrogen atoms, respectively. The parameters in eq 1 were optimized for the present four-site model to yield reasonable energetic and structural results for the gas-phase bimolecular complexes and for the liquid at its boiling point (-33.35°C). The Lennard-Jones parameters for the hydrogen atoms were chosen to be zero, while the parameters for the nitrogen–nitrogen interactions were optimized to give good agreement between the computed and experimental liquid densities. The final parameters are listed in Table II, along with those of the FHMK model. As usual, exact accord between the dipole moment based upon the atomic charges and the experimental value in the gas phase was not sought because the primary emphasis was to reproduce liquid thermodynamic properties. The present charge model yields a dipole moment of 1.88 D, which may be compared to the experimental value of 1.47 D and that of 1.50 D predicted by the FHMK model.¹⁵ Note that it is often necessary to use charges that yield dipole moments ca. 15–30% greater than for an isolated molecule in effective pairwise potentials for simulation of polar liquids.¹⁶

Monte Carlo Simulations. Monte Carlo statistical mechanics simulations were carried out for liquid ammonia using the present four-site potential and the FHMK model using BOSS.¹⁷ The system consists of 267 ammonia monomers in a cubic box of about $22 \times 22 \times 22 \text{\AA}^3$. The isothermal–isobaric (NPT) ensemble at -33.35°C and 1 atm was used along with the periodic boundary conditions in the Metropolis sampling. The boiling point temperature is the typical condition for performing organic reactions in liquid ammonia. Intermolecular interactions were smoothly reduced to zero at spherical cutoff distances between 8.5 and 9.0 \AA based upon the nitrogen separation of two monomers. A correction was made for the Lennard-Jones potential neglected beyond the cutoff radius, which as in previous studies was found to lower the total energy by ca. 2%.¹⁸ There is no generally accepted procedures for correcting the long-range electrostatic interactions. The contribution is expected to be small since it has been found from previous simulations that there is little size dependency of the computed properties for liquid water.¹⁹

In each simulation, new configurations were generated by randomly translating a randomly selected ammonia molecule in all three Cartesian directions, and rotating it around a randomly chosen axis. The range for the translations and rotations were $\pm 0.2 \text{\AA}$ and $\pm 20^\circ$, which yielded an acceptance rate of roughly

**Figure 1.** Structures considered for the bimolecular complexes of ammonia.

45% for new configurations. Volume fluctuations were attempted on every 1625 configurations within the range of $\pm 390 \text{\AA}^3$ by scaling all monomer coordinates. Each simulation was equilibrated for at least 1.5×10^6 configurations followed by 3×10^6 configurations for averaging. All calculations were executed on a Titan 3000 computer in our laboratory.

Results and Discussion

Bimolecular Complexes. Ab initio calculations have been carried out to study the hydrogen bonding interactions in ammonia dimer and ammonia–water complexes by several research groups. The most extensive work is by Del Bene and by Scheiner and co-workers who have located the minimum hydrogen-bonding complexes by using the 6-31G(d) basis set.^{7,8a} Energy computations including electron correlations using MP4/6-31+G(2d,2p) indicated that diffuse functions on non-hydrogen atoms are the most important in these calculations.^{7a} On the experimental side, there has been strong evidence that ammonia is an excellent hydrogen bond acceptor with a nearly colinear hydrogen bond; however, the hydrogen-bond-donating ability of NH_3 was predicted to be very poor.^{2,3} Although estimates of about -4.5 kcal/mol for the ammonia dimer have been reported,²⁰ recent laser dissociation experiments suggested that the binding energies for ammonia complexes are less than 2.8 kcal/mol .^{2,3a}

We have used the Gaussian 90 program to optimize six low-energy bimolecular complexes of ammonia with the 6-31+G(d) basis set.^{21,22} The structures are illustrated in Figure 1. In these calculations, the monomer geometries were held fixed at the 6-31+G(d) values. The 6-31+G(d) basis functions have been shown to yield excellent results for hydrogen bonding complexes.^{7,22} In Table III, the results of the partial 6-31+G(d) optimizations are compared with those of Del Bene by including electron correlation corrections. The findings for these complexes optimized with the empirical potential functions used in the Monte Carlo simulations are also given in this table.

Both the 6-31+G(d) calculations and the empirical potential function concur that the ammonia–water complex **D** forms the strongest hydrogen bond. The optimized geometry shows that the hydrogen bond is nearly linear along the N–O axis with slight deviations of a few degrees in these calculations. The optimal N–O separation is 3.04 \AA for the 6-31+G(d) structure, 2.94 \AA for the FHMK model, and 2.85 \AA for the present model. This may be compared with the experimental value of 3.27 \AA from microwave spectroscopy data.^{3c} The predicted binding energy for **D** is -6.2 kcal/mol with the 6-31+G(d) basis set, -5.4 kcal/mol using the FHMK potential, and -6.5 kcal/mol using our model. These results are in good accord with the best theoretical estimate of -6.6 kcal/mol at the MP4/6-31+G(2d,2p) level.^{7,8} For complexes **A–C**, which all involve ammonia hydrogen bond donors, the binding energies are much smaller than in **D**. The **C**, structure **A** was predicted to be the global minimum for the

TABLE III: Calculated Hydrogen-Bond Energies (kcal/mol) and Geometries for Bimolecular Complexes^a

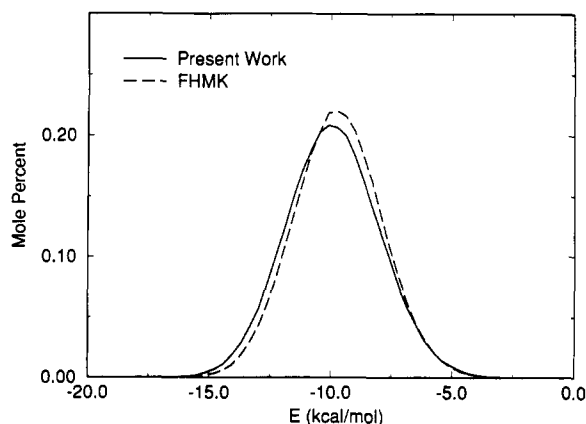
species		MP3/		FHMK	this work
		6-31+G(d)	6-31+G(2d,2p) ^b		
A	R_{NN}	3.38	3.38	3.25	3.16
	$\angle \text{NNH}$	10	10	-3 ^c	7
	ΔE	-2.75	-2.99	-2.69	-2.96
B	R_{NN}	3.31	3.27	3.26	3.15
	$\angle \text{NNH}$	43	41	38	35
	ΔE	-2.52	-3.00	-2.44	-2.87
C	R_{NO}	3.30		3.04	3.02
	$\angle \text{NOH}$	6		8	5
	ΔE	-2.37		-3.04	-3.11
D	R_{NO}	3.04	3.04	2.94	2.85
	$\angle \text{NOH}$	1	0	-2 ^c	-2 ^c
	ΔE	-6.24	-6.3	-5.27	-6.44
E	R_{NN}			3.17	
	$\angle \text{NNH}$			2	
	ΔE			-2.14	
F	R_{NO}			2.85	
	$\angle \text{NOH}$			2	
	ΔE			-3.96	

^a Energies are given in kilocalories per mole. Units for distances and angles are angstroms and angles, respectively. ^b Reference 7a,b with 6-31G(d) geometries. ^c Negative angles imply that the N-H bond is on the opposite side of the N-N axis as shown in Figure 1.

ammonia dimer from ab initio calculations, while **B** corresponds to the transition state for the interchange of donor and acceptor monomers.⁷ However, the barrier height is only 0.2 kcal/mol, and inclusion of electron correlation corrections yields similar results.⁷ The computed interaction energies are -2.7, -2.5, and -2.4 kcal/mol for **A**, **B**, and **C**, respectively, using the 6-31+G(d) basis set, which are consistent with the estimate by Klemperer and co-workers.^{2,3} The interaction energies computed with the empirical potentials are in reasonable agreement with the ab initio estimates. For complex **C**, both empirical models predict greater interaction energies than the corresponding ab initio value.

There has been much discussion on the structure of ammonia dimer in the gas phase.²⁻⁸ As pointed out previously, neither of the structures **A** nor **B** may be assigned to the experimental configuration because the computed dipole moments for **A** and **B** do not agree with the experimental value.^{2,3,7} In view of the shallow potential surface of the ammonia dimer which is further complicated by the quantum mechanical tunneling effect, it has been suggested that there is unlikely to exist a unique equilibrium structure in the gas phase.⁴ Our present potential function, which is designed to reproduce condensed-phase thermodynamic properties, appears to agree with these general features of the intermolecular interactions. Additional justification of our model is provided by fluid simulations presented below.

Structures **E** and **F** were considered because similar arrangements were observed in the liquid simulation of ammonia using the FHMK potential (vide infra). Intuitively, hydrogen bonding interactions are not expected in **E** and **F** for electrostatic reasons, and this expectation has been confirmed by ab initio calculations. Specifically, when the nitrogen or oxygen in the donor molecule is constrained along the C_{3v} axis of the receptor monomer, the interaction energies for **E** and **F** are positive and no minima can be located at the 6-31+G(d) level. Without the geometrical constraint, **E** and **F** were optimized to give structures **A** and **D**. With the present potential function the same conclusion was reached. However, geometry optimizations using the FHMK potential yielded two minima on the potential surfaces for **E** and **F** with competitive binding energies of -2.14 and -3.96 kcal/mol. This can be attributed to the placement of the large negative charge in the five-site model. Here, instead of using the position of the lone pair in ammonia to carry the negative charge, the virtual site was placed toward the three hydrogen atoms, resulting in unrealistic results. The structural features are expected to fully transfer into the liquid in simulations using the FHMK potential.

**Figure 2.** Distributions of total intermolecular bonding energies for liquid ammonia. Bonding energies are given in kcal/mol. The units for the ordinate are mole percent per kcal/mol.**TABLE IV: Thermodynamic Results for Liquid Ammonia at -33.35 °C**

	FHMK model	this work	expt ^a
V , Å ³	39.7 ± 0.1	39.1 ± 0.1	41.5
d , g/cm ³	0.712 ± 0.002	0.723 ± 0.002	0.682
$-E_i(l)$, kcal/mol	4.97 ± 0.01	5.05 ± 0.01	5.18
$\Delta H^\circ_{\text{vap}}$, kcal/mol	5.45 ± 0.01	5.53 ± 0.01	5.66
ΔH_{vap} , kcal/mol	5.37 ± 0.01	5.45 ± 0.01	5.58
C_p , cal/K-mol	21.6 ± 1.8	20.9 ± 1.7	18.0
α , 10 ⁵ deg ⁻¹	145 ± 21	221 ± 33	181
κ , 10 ⁶ atm ⁻¹	51 ± 6	86 ± 11	91

^a Reference 24.

Thermodynamics. The computed and experimental thermodynamic results are given in Table IV. The standard errors ($\pm 1 \sigma$) for the computed quantities were obtained from the fluctuations of separate averages over blocks of 1×10^5 configurations. The computed total intermolecular potential energy of liquid ammonia, $E_i(l)$, and the heat of vaporization to the ideal gas, $\Delta H^\circ_{\text{vap}}$, is related by

$$\Delta H^\circ_{\text{vap}} = -E_i(l) + RT \quad (2)$$

where $\Delta H^\circ_{\text{vap}}$ can be evaluated from the experimental heat of vaporization to the real gas, ΔH_{vap} , via the enthalpy departure function ($H^\circ - H$):

$$\Delta H^\circ_{\text{vap}} = \Delta H_{\text{vap}} + (H^\circ - H) \quad (3)$$

The correction for the nonideality of the ammonia gas can be obtained through the virial equation of state

$$(H^\circ - H) = \frac{RT}{V} \left(T \frac{dB(T)}{dT} - B(T) \right) \quad (4)$$

where $B(T)$ is the second virial coefficient. Using the empirical equation and parameters of Keyes for $B(T)$ in the temperature range -35 to 325 °C,²³ the deviation of heat of vaporization between the real and ideal gases is 0.076 kcal/mol at -33.35 °C.¹⁰ The correction has been used to obtain the experimental $\Delta H^\circ_{\text{vap}}$ and $E_i(l)$, and the computed ΔH_{vap} in Table IV. The calculated heats of vaporization using both the FHMK and our new potential functions are within 4% of the experimental value.²⁴ Interestingly, the results are nearly identical from the two theoretical models, indicating that there are no particular advantages to use a five-site model over the present four-site representation of ammonia. Nevertheless, the apparent agreement between the two empirical models is surprising in view of the difference in the predicted structures for bimolecular complexes (vide supra).

The distributions of the total binding energies for the monomers in the liquid are shown in Figure 2. Note that the average energies from the distributions are twice the $E_i(l)$ values in Table IV. The ammonia molecules experience a smoothly distributed spectrum

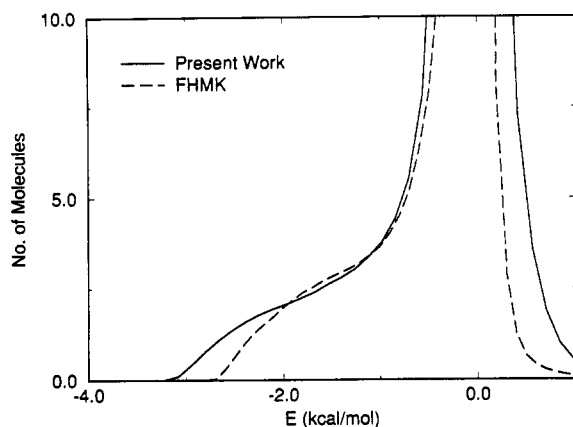


Figure 3. Distributions of individual interaction energies between molecules in liquid ammonia. Energies are in kcal/mol. The units for the ordinate are number of molecules per kcal/mol.

of energetic environment covering a 12 kcal/mol range. The distributions are similar for the two theoretical models investigated, while some details on the dimer interactions are revealed in the distributions of pair-interaction energies displayed in Figure 3. The low-energy bands correspond to the hydrogen-bonding interactions in liquid ammonia, but clearly the distributions are not well-defined as opposed to that for liquid water, which shows definite hydrogen bonding regions.¹⁶ This of course is due to the much weaker interactions for ammonia dimer than for the water dimer.¹⁶ Most interactions in the liquid involve distant bulk molecules and appear in the spike centered at 0 kcal/mol. Although the number of hydrogen bonds can in principle be estimated from the energy pair distributions, it is difficult to deconvolute the smooth shoulders into specific contributions in Figure 3. Alternate measures of coordination numbers are provided below from analysis of the radial distribution functions and hydrogen bonds.

The energy distributions shown in Figure 2 are the primary indicator for the intermolecular contribution to the liquid heat capacity, which is computed from the enthalpy fluctuations:

$$C_p(l) = \frac{\langle H_l(l)^2 \rangle - \langle H_l(l) \rangle^2}{RT} \quad (5)$$

where $H_l(l) = E_l(l) + PV$, and P and V are the pressure and volume of the liquid. The total heat capacity of the liquid is then estimated from $C_p(l)$ plus an intramolecular term taken as the ideal gas value,²⁵ $C_p(g)$, (8.3 cal/(K mol)) minus R for the PV component. The computed results agree well with the experimental data.²⁴

Other quantities that were calculated from the fluctuations involving the volume and enthalpy include the coefficient of thermal expansion (α) and the isothermal compressibility (κ). The computed α values for liquid ammonia are 221×10^{-5} and $145 \times 10^{-5} \text{ K}^{-1}$ from the four- and five-site models, respectively, which may be compared with the experimental value of $181 \times 10^{-5} \text{ K}^{-1}$.²⁴ The estimated κ 's are 86×10^{-6} (four-site model) and $51 \times 10^{-6} \text{ atm}^{-1}$ (FHKM model), while the experimental number is $91 \times 10^{-6} \text{ atm}^{-1}$.²⁴ These quantities converge very slowly in the Monte Carlo simulations. To increase the accuracy, much longer simulations are needed.

Finally, the computed molecular volumes and liquid densities are compared with the experimental data in Table IV. Again, both theoretical models yielded similar results that differ from the experimental value by less than 6%.²⁴ Considering the relatively low density of liquid ammonia at its boiling point, the agreement is good and supports the choice of the Lennard-Jones parameters.

Radial Distribution Functions. The structures of the liquid can be characterized by radial distribution functions (rdf), $g_{xy}(r)$, which give the probability of finding an atom of type y a distance r from an atom of type x . Peaks in the rdfs are often assigned

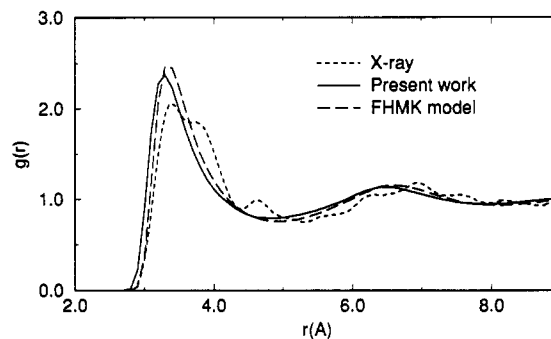


Figure 4. NN radial distribution functions for liquid ammonia. Distances are in angstroms throughout.

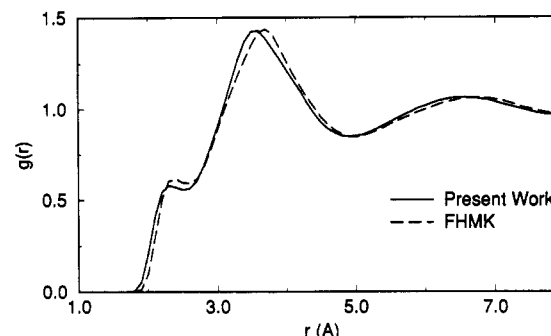


Figure 5. NH radial distribution functions for liquid ammonia.

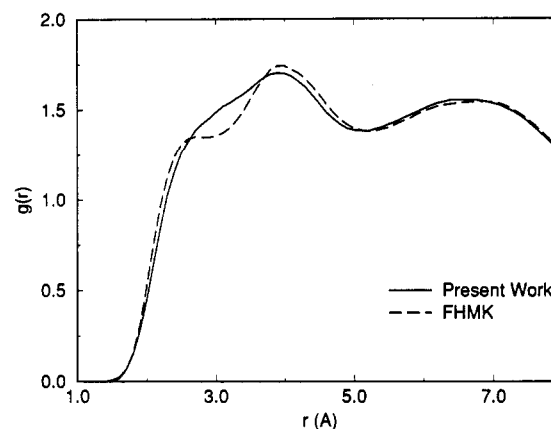


Figure 6. HH radial distribution functions for liquid ammonia.

to hydrogen bonding or solvation shells in polar liquids. However, since the angular distributions are averaged into the rdfs, it is not possible to obtain specific information on the orientations in hydrogen-bonding interactions and only the number of nearest neighbors can be derived from the rdfs.

The corresponding rdfs computed at -33.35°C using the present and the FHKM models are compared in Figures 4–6. The results for g_{NN} are shown in Figure 4 along with the X-ray data by Narten at 4°C .²⁶ The computed NN rdfs compare favorably with the experimental data, although the double-band feature suggested by the pronounced shoulder in the experimental curve at 3.7 Å is not predicted, and the positions of the first peaks are about 0.2 Å shorter than the X-ray data. The FHKM model has somewhat closer agreement with the experimental first peak position than the present four-site model. It should be mentioned that the location of the first peak in $g_{OO}(r)$ for liquid water predicted by empirical potential functions is also about 0.1 – 0.2 Å shorter than neutron diffraction data.¹⁶ There are also clearly identifiable second peaks at 6.5 – 6.6 Å in the NN rdfs, which are in accord with the experimental data at 4°C . Integration of the first peak to the minimum at 4.9 Å yielded an average of 12.3 and 12.2 neighbors with our four-site model and the FHKM model, respectively. This may be compared with the experimental figure of 12 at 5 Å .

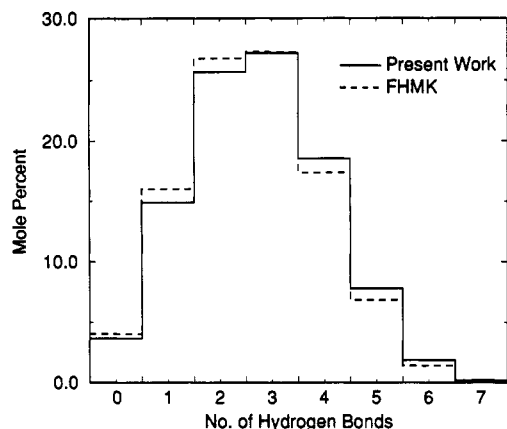


Figure 7. Distributions of coordination numbers for hydrogen-bonding neighbors from the two theoretical models. The units for the ordinate are mole percent. A hydrogen bond is defined by a separation distance of 2.65 Å between the donor and acceptor atoms.

The NH and HH rdfs are depicted in Figures 5 and 6. The results are nearly identical for the NH distribution from the two models, whereas the FHMK model showed more structured features at about 3 Å in the HH distribution. Experimental data are not available for guidance in these cases. The small peak at 2.3 Å in the NH rdfs has been noted before and may be assigned to the $\text{N}\cdots\text{H}-\text{N}$ hydrogen bonds.¹⁰⁻¹⁴ This distance agrees well with hydrogen-bond length in the NH_3 crystal (2.37 Å).²⁷ Integration of the bands to their minima at 2.5 Å for the four-site model and at 2.6 Å for the FHMK model revealed 1.5 and 1.7 hydrogens per nitrogen, respectively, which suggest that each monomer in the liquid forms about 3 hydrogen bonds. A thorough analysis of the hydrogen bonding is presented below.

Hydrogen-Bonding Analyses and Liquid Structure. The hydrogen bonding in liquid ammonia was further analyzed by using the configurations saved every 5000 attempted moves during the Monte Carlo simulations. In general, hydrogen bonds can be defined by an energetic criterion based upon the positions of the minima in the energy pair distributions, by geometrical considerations available from the positions of minima in the rdfs, or by a combination of the two.²⁸ Since the intermolecular interactions are weak for liquid ammonia, resulting in vaguely defined maxima and minima in the energy pair distributions (Figure 3), energetic criterion did not seem to be the best choice for defining hydrogen bonds in the present study. Consequently, a geometrical criterion was adopted such that the ammonia-ammonia hydrogen bond was defined by a distance of 2.65 Å or less between the hydrogen and nitrogen atoms in two monomers. Angular restrictions were not imposed in order to analyze the distributions of hydrogen-bond angles.

The distribution of hydrogen-bond numbers are shown in Figure 7. There are on average 2.74 and 2.65 hydrogen bonds for each ammonia from simulations using the present and the FHMK models, respectively. This is in good accord with the value of about 3 obtained by integrating the NH rdfs.²⁶ Most monomers (ca. 54%) were predicted to form two or three hydrogen bonds from both theoretical models, while about 15% (16%) and 19% (17%) share one or four hydrogen bonds, respectively, using the present four-site model (the FHMK model). Furthermore, there are about 4% free monomer and about 10% ammonia forming more than four hydrogen bonds in the liquid. Thus, the present results are consistent with the picture of hydrogen-bonding chains in the liquid predicted by Jorgensen and Ibrahim,¹⁰ though, in that study the predicted number of hydrogen bonds was about two per monomer. A Raman study of liquid ammonia solutions also indicated that liquid ammonia consisted of linear polymeric hydrogen-bonded monomers.²⁹ Finally, of the 2.7 hydrogen bonds per monomer, the hydrogen-bonding analysis shows that there are on average 0.16 ammonia dimers that form hydrogen bonds

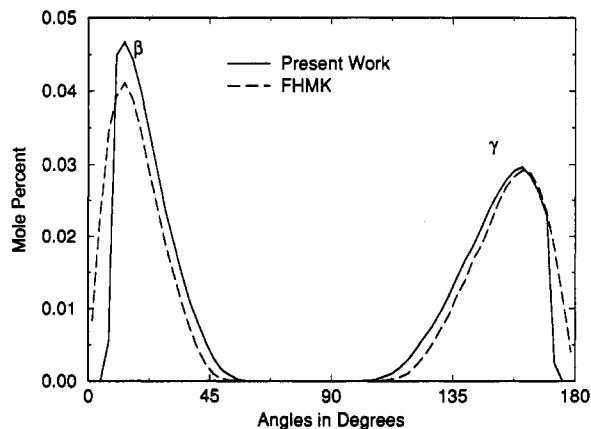
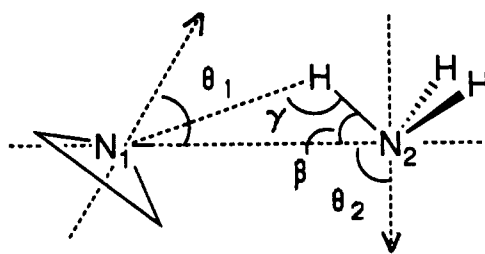


Figure 8. Distributions of the hydrogen bond angle β ($\angle\text{N}\cdots\text{NH}$) and γ ($\angle\text{N}\cdots\text{HN}$) between hydrogen-bonded ammonia molecules in the liquid. The units for the y axis are mole percent per degree.

from both monomers (cyclic structures). This is about 6% of the total number of hydrogen-bonded complexes in the liquid.

The distribution of hydrogen-bond angles are displayed in Figure 8, in which β is the $\text{N}\cdots\text{N}-\text{H}$ angle and γ is the $\text{N}\cdots\text{H}-\text{N}$ angle. Both potential functions showed preference for values near 0° and 180°, respectively. The maximum β values occur at 14° both with our four-site model and the FHMK model, while the maxima for γ are 160°. Although the results seem to indicate that hydrogen bonds in the liquid are significantly bent (ca. 20°) in the liquid, the intrinsic preference for linearity should be described, and is confirmed by the probability function obtained by dividing the distributions in Figure 8 by $\sin \beta$ or $\sin \gamma$ to correct the volume-element contribution.¹⁰ The results may also be compared with the findings from the crystal structure of ammonia, in which the $\text{N}\cdots\text{H}-\text{N}$ angle was determined to be 164.2°,²⁷ in good accord with the present results for the liquid. The previous study by Jorgensen and Ibrahim using an ab initio STO-3G potential predicted β and γ values of 25° and 167°, respectively.¹⁰

The structures of the hydrogen-bonded complexes in the liquid are further characterized by the angle distributions displayed in Figures 9 and 10. Angles θ_1 and θ_2 for the dimer complex are defined as follows:



16

Here, the acceptor NH_3 monomer is drawn as a cone to indicate that the positions of the hydrogen atoms are not specifically defined, while the hydrogens of the donor NH_3 are specified to define the hydrogen bonds in the calculation. The orientation of the donor nitrogen atoms or the $\text{N}\cdots\text{H}-\text{N}$ angle (γ) has been characterized above in Figure 8, and roughly linear hydrogen-bond angles with a maximum distribution at about 160° were obtained from both theoretical models. However, it should be noted that the dihedral angle of the symmetry axes of the NH_3 monomers connected by the two nitrogens is not defined and is shown coplanar for convenience in the above figure.

Figure 9 shows that the most probable structures for the ammonia dimers in the liquid occur at about $\theta_1 = 40^\circ$ and $\theta_2 = 110^\circ$ with our four-site model. Note that the optimal geometry

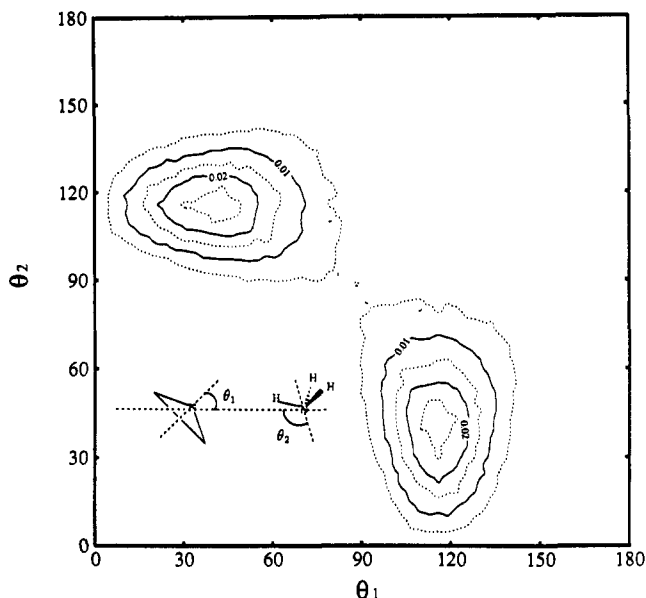


Figure 9. Distributions of the angles θ_1 and θ_2 defining the relative orientations of hydrogen-bonded monomers (see text) from the Monte Carlo simulation with the present four-site potential function. Contour levels are 0.005 mol% per degree².

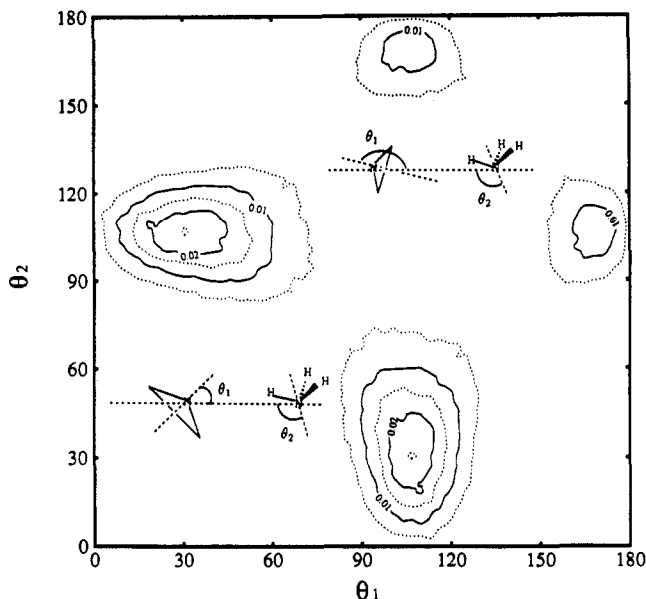


Figure 10. Distributions of the angles θ_1 and θ_2 defining the relative orientations of hydrogen-bonded monomers (see text) from the Monte Carlo simulation with the FHMK potential function. Contour levels are 0.005 mol% per degree².

for the cyclic dimer in the gas phase corresponds to the point at about (70°, 70°). Obviously, no noticeable distributions were observed in the present simulations. The most significant difference between the present work and the FHMK model is the appearance of a second "hydrogen-bonding" region with the FHMK model (Figure 10). This is particularly surprising in view of the agreement for the computed thermodynamic properties between the two theoretical models. However, further examination of the bimolecular complexes revealed an unrealistic minimum (Table III, E) for the ammonia dimer in the gas phase using the FHMK model, which is fully transferred into the liquid simulations. The second band is assigned to the structure exemplified by E in Figure 1, representing donation of a hydrogen bond to the opposite side of the lone pair (Figure 10). Integration of this band shows that it contains ca. 24% of the total hydrogen bonds in the liquid using the FHMK model. In contrast, both *ab initio* calculations and the present four-site model yielded no

stable structures for E and F. Thus, the second band did not occur in Figure 9 for our four-site potential.

The difference in the structural details observed here is particularly noteworthy because the two models yielded virtually identical thermodynamic properties and radial distribution functions for the liquid, all in good agreement with the available experimental data (*vide supra*). The findings of this study emphasize the importance of a detailed consideration of bimolecular interactions in developing potential functions for fluid simulations and suggest that erroneous results might be obtained if the potential functions are fitted to reproduce condensed-phase properties alone.

In closing, stereoviews of the last configurations from the simulations of liquid ammonia using our four-site potential and the FHMK potential are given in Figures 11 and 12, respectively. In viewing the plots, the periodic boundary conditions must be invoked, so that molecules near one side also interact with molecules on the opposite face. For clarity, monomers in the bottom half of the cubic box have been removed.

The structural notions discussed above are evident in the stereoplots. In Figure 11, chains of hydrogen bonds are widespread in the liquid modeled by the four-site potential. The darkened molecules feature a chain of hydrogen bonded monomers, in which hydrogen-bond relays and branchings (Y junctions) of the chains are apparent. Note that a cyclic dimer is clearly seen at the upper left portion of the chain, while a trimer is also apparent at the opposite end. The FHMK ammonia displayed in Figure 12, however, exhibits remarkably different features. The most dramatic is the occurrence of the dimer structures depicted by E (Figure 1), two of which are highlighted in the plot, one in the middle of a chain of monomers, and the other shown separately. Although chains of hydrogen bonds are seen in Figure 12, they are clearly not as widespread as those in Figure 11. In addition, the E-type structures are seen to participate in forming the monomer chains as indicated in Figure 12. Of course, statistical fluctuations in the fluid phase would allow the existence of the E-type structures; however, the high population predicted by the FHMK model (ca. 24%) seems to be counterintuitive to the nature of hydrogen bonding interactions. This discrepancy may be resolved by comparison with accurate experimental *rdfs* for $g_{HH}(r)$ and $g_{NH}(r)$ from neutron diffraction measurements, which are not presently available.

Conclusion

Monte Carlo statistical mechanics simulations of liquid ammonia have been carried out using the four-site model developed in the present study. The potential function for NH₃ is shown to exhibit good success in reproducing the experimental heat of vaporization and liquid density, whereas the computed radial distribution function for the NN pair was in accord with the X-ray data. Detailed analyses of hydrogen-bonding interactions in the liquid along with examination of bimolecular complexes of the ammonia dimer and complexes with water suggest that each monomer on average participates in about three hydrogen bonds. This leads to the formation of winding chains of hydrogen-bonded monomers in the liquid. The preference for linear hydrogen bonds is assured from the distributions of hydrogen-bond angles, although the dimer interaction energies are weak in liquid ammonia. Cyclic structures were found to constitute about 6% of the total hydrogen-bonded dimers in the liquid, while trimer structures are also seen from the graphics analysis. These structural features of liquid ammonia are in qualitative agreement with the prediction by Jorgensen and Ibrahim using a STO-3G derived potential function.¹⁰

Comparison was made with the results obtained using the five-site model developed by Ferrario et al. (FHMK model).^{11,12} Although the computed heat of vaporization, liquid density, and the radial distribution functions are in good accord with the present results and experimental data, to our surprise, significant

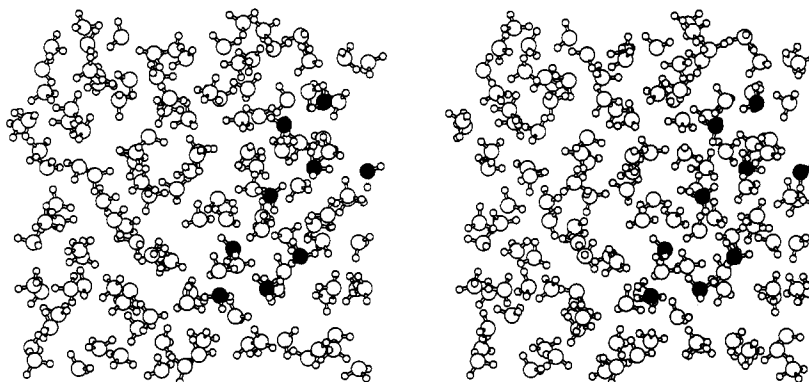


Figure 11. Stereoplot of a configuration from the Monte Carlo simulation of liquid ammonia with the present model.

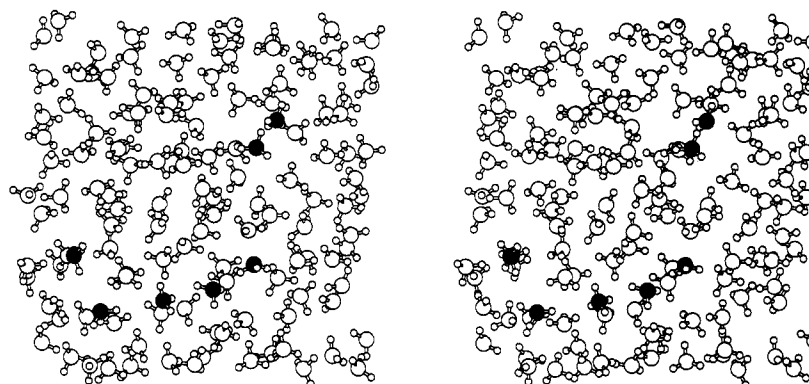


Figure 12. Stereoplot of a configuration from the Monte Carlo simulation of liquid ammonia with the FHMK model.

difference in dimer and liquid structures exists between the two theoretical models. The departure is characterized by the occurrence of unrealistic dimer structures with donation of hydrogen bonds to the opposite side of the ammonia lone pair in the FHMK liquid. In contrast, both *ab initio* calculations and the present four-site model yielded no stable complexes for these structures. The findings emphasize the importance of consideration of bimolecular interactions in developing potential functions for fluid simulations³⁰ and suggest that erroneous results might be obtained if the potential functions are fitted to reproduce condensed-phase properties alone.

Acknowledgment. Gratitude is expressed to the National Institutes of Health (GM46736) for support of this research.

References and Notes

- (1) Cotton, A. F.; Wilkinson, G. *Advanced Inorganic Chemistry: A Comprehensive Text*, 4th Ed.; John Wiley Sons: New York, 1980; p 415.
- (2) Nelson, D. D., Jr.; Fraser, G. T.; Klemperer, W. *Science* **1987**, *238*, 1670.
- (3) (a) Fraser, G. T.; Nelson, D. D.; Charo, A.; Klemperer, W. *J. Chem. Phys.* **1985**, *82*, 2535. (b) Nelson, D. D., Jr.; Fraser, G. T.; Klemperer, W. *J. Chem. Phys.* **1985**, *83*, 6201. (c) Nelson, D. D., Jr.; Klemperer, W. *J. Chem. Phys.* **1987**, *139*. (d) Nelson, D. D., Jr.; Klemperer, W.; Fraser, G. T.; Lovas, F. J.; Suenram, R. D. *J. Chem. Phys.* **1987**, *87*, 6364. (e) Stockman, P. A.; Bumgarner, R. E.; Suzuki, S.; Blake, G. A. *J. Chem. Phys.* **1992**, *96*, 2496. (f) Odutola, J. A.; Dyke, D. R.; Howard, B. J.; Muentner, J. S. *J. Chem. Phys.* **1979**, *70*, 4884.
- (4) Pimentel, G. C.; McClellan, A. L. *The Hydrogen Bond*; Freeman: San Francisco, 1960.
- (5) (a) Perchard, J.-P.; Bohn, R. B.; Andrews, L. *J. Phys. Chem.* **1991**, *95*, 2707. (b) Bohm, R. B.; Andrews, L. *J. Phys. Chem.* **1991**, *95*, 9707. (c) Im, H. S.; Gaussian, V. H.; Bernstein, E. R. *J. Phys. Chem.* **1990**, *94*, 222.
- (6) (a) Loeser, J. G.; Schmittenmaier, C. A.; Cohen, R. C.; Elrod, M. J.; Steyert, D. W.; Saykally, R. J.; Bumgarner, R. E.; Blake, G. A. *J. Chem. Phys.* **1992**, *97*, 4727. (b) van Bladel, J. W. I.; van der Avoird, A.; Wormer, P. E. S.; Saykally, R. J. *J. Chem. Phys.* **1992**, *97*, 4750.
- (7) (a) Del Bene, J. E. *J. Phys. Chem.* **1988**, *92*, 2874. (b) Del Bene, J. E. *J. Chem. Phys.* **1987**, *86*, 2110. (c) Frisch, M. J.; Del Bene, J. E.; Binkley, J. S.; Schaefer, H. F., III *J. Chem. Phys.* **1986**, *84*, 2279. (d) Del Bene, J. E.; Frisch, M. J.; Pople, J. A. *J. Phys. Chem.* **1985**, *89*, 3669. (e) Frisch, M. J.; Pople, J. A.; Del Bene, J. E. *J. Phys. Chem.* **1985**, *89*, 3664.
- (8) (a) Latajka, Z.; Scheiner, S. *J. Phys. Chem.* **1990**, *94*, 217. (b) Dykstra, C. E.; Andrews, L. *J. Chem. Phys.* **1990**, *92*, 6043. (c) Hassett, D. M.; Marsden, C. J.; Smith, B. J. *Chem. Phys. Lett.* **1991**, *183*, 449.
- (9) Gao, J. *J. Am. Chem. Soc.* **1991**, *113*, 7796.
- (10) Jorgensen, W. J.; Ibrahim, M. *J. Am. Chem. Soc.* **1980**, *102*, 3309.
- (11) (a) McDonald, I. R.; Klein, M. L. *J. Chem. Phys.* **1976**, *64*, 4709. (b) Duquette, G.; Ellis, T. H.; Scoles, G.; Watts, R. O.; Klein, M. L. *J. Chem. Phys.* **1978**, *68*, 2544. (c) Hinchliffe, A.; Bounda, D. G.; Klein, M. L.; McDonald, I. R.; Righini, R. *J. Chem. Phys.* **1981**, *74*, 1121. (d) Impey, R. W.; Klein, M. L. *Chem. Phys. Lett.* **1984**, *104*, 579.
- (12) Ferrario, M.; Haughney, M.; McDonald, I. R.; Klein, M. L. *J. Chem. Phys.* **1990**, *93*, 5156. The potential for ammonia reported in this paper is a modified version of that of ref 11d.
- (13) (a) Scheraga, H. A.; Kincaid, R. H. *J. Phys. Chem.* **1962**, *66*, 833. (b) Sagarik, K. P.; Ahlrichs, R.; Brode, S. *Mol. Phys.* **1966**, *57*, 1247. (c) Mansour, K. A.; Murad, S. *Fluid Phase Equil.* **1987**, *37*, 305. (d) Mansour, K. A.; Murad, S.; Powles, J. G. *Mol. Phys.* **1988**, *65*, 785.
- (14) Benedict, W. S.; Plyler, E., K. *Can. J. Chem.* **1957**, *35*, 1235.
- (15) Nelson, R. D.; Lide, D. R.; Maryott, A. A. *Natl. Stand. Ref. Data Ser., Natl. Bur. Stand.* **1967**, No. 10.
- (16) Jorgensen, W. L.; ChandraSekhar, J.; Madura, J. D.; Impey, R. W.; Klein, M. L. *J. Chem. Phys.* **1983**, *79*, 926.
- (17) Jorgensen, W. L. *BOSS, Version 2.9*; Department of Chemistry, Yale University, 1990.
- (18) Jorgensen, W. L.; Madura, J. D.; Swenson, C. J. *J. Am. Chem. Soc.* **1984**, *106*, 6638.
- (19) Jorgensen, W. L.; Madura, J. D. *Mol. Phys.* **1985**, *56*, 1381.
- (20) (a) Lowder, J. E. *J. Quant. Spectrosc. Radiat. Transfer* **1970**, *10*, 1085. (b) Lambert, J. D.; Strong, E. D. T. *Proc. R. Soc. London, Ser. A* **1950**, *200*, 566.
- (21) Frisch, M. J.; Head-Gordon, M.; Trucks, G. W.; Foresman, J. B.; Schlegel, H. B.; Raghavachari, K.; Robb, M.; Binkley, J. S.; Gonzalez, C.; Defrees, D. J.; Fox, D. J.; Whiteside, R. A.; Seeger, R.; Melius, C. F.; Baker, J.; Martin, R. L.; Kahn, L. R.; Stewart, J. J. P.; Topiol, S.; Pople, J. A. *Gaussian 90, Revision J*; Gaussian, Inc., Pittsburgh PA, 1990.
- (22) Hehre, W. J.; Radom, L.; Schleyer, P. v. R.; Pople, J. A. *Ab Initio Molecular Orbital Theory*; Wiley: New York, 1986.
- (23) Keyes, F. G. *J. Am. Chem. Soc.* **1938**, *60*, 1761.
- (24) Haar, L.; Gallagher, J. S. *J. Phys. Chem. Ref. Data* **1978**, *7*, 635.
- (25) Chase, M. W., Jr.; Davies, C. A.; Downey, J. R., Jr.; Frurip, D. J.; McDonald, R. A.; Syverud, A. N. *JANAF Thermochemical Tables*; Kynoch Press: Birmingham, UK, 1986; Vol. 14.
- (26) Narten, A. H. *J. Chem. Phys.* **1977**, *66*, 3117.
- (27) (a) Reed, J. W.; Harris, P. M. *J. Chem. Phys.* **1961**, *35*, 1730. (b) Olovsson, I.; Templeton, D. H. *Acta Crystallogr.* **1959**, *12*, 827.
- (28) Gao, J.; Jorgensen, W. L. *J. Phys. Chem.* **1988**, *92*, 5813.
- (29) Lemley, A. T.; Roberts, J. H.; Plowman, K. R.; Lagowski, J. J. *J. Phys. Chem.* **1977**, *77*, 2185.
- (30) Jorgensen, W. L.; Tirado-Rives, J. *J. Am. Chem. Soc.* **1988**, *110*, 1657.